Removal of arsenic contaminants from water using iron oxide nanoparticles by inductively coupled plasma mass spectrometery

Syeda Sara Hassan (ssarahassan@gmail.com)
MUET: Mehran University of Engineering & Technology https://orcid.org/0000-0003-1557-8385
Syed Shane Zehra
MUET: Mehran University of Engineering & Technology
Zubair Ahmed
MUET: Mehran University of Engineering & Technology
MOHAMMAD YOUNIS Younis TALPUR
University of Sindh
Sallahuddin Panhwar
Balochistan University of Engineering and Technology Khuzdar

Research Article

Keywords: Arsenic, water sources, iron oxide nano-adsorbent, ICP-MS, removal efficiency

Posted Date: March 28th, 2022

DOI: https://doi.org/10.21203/rs.3.rs-1469404/v1

Abstract

ו The adsorption capacity of arsenic on the prepared novel iron oxide nanoparticles was 1.96 mg/g having higher surface area with excellent catalytic degradation property.

ו The adsorption dataset best fits in the Langmuir model (pseudo-second-order model).

ו To check the removal efficiency of arsenic by iron oxide magnetite nano catalyst (adsorbent) on real water samples was 81.09% and synthetic water prepared on laboratory was 99.8% tested by Inductively couple plasma mass spectrometry (ICP-MS) instrument.

1 Introduction

Groundwater is considered as fundamental source of water, which can be consumed, and more than one-third of the population is almost dependent on it for drinking purposes (Xing et al. **2013;** Emenike et al. **2017a**). Moreover, due to scarcity of surface water people rely on the groundwater, which further results in causing overexploitation. Numerous researchers investigated the condition of groundwater from the different countries of the world to know more about the contamination of the groundwater (Khan et al. **2013**; Li et al. **2014a**; Li et al. **2014b**; Malassa et al. **2014**). Arsenic is considered as one of the most lethal, toxic metalloid and carcinogenic. This word arsenic comes from the Greek word arsenikon, which means potent (Choong et al. **2007**) and arsenikon is taken from a Persian word “Zarnikh”, meaning yellow orpiment (Mudhoo et al. **2011**). According to the United States Environmental Protection Agency (USEPA) and World Health Organization, the permissible limit of arsenic in the water is 10 µg/L (Hassan et al. **2012**; Gul et al. **2020**) whereas many developing and underdeveloped countries have the limit of 50 µg/L (Mushtaq et al. **2018**; Nickson et al. **2005**). Arsenic (As) is considered a ubiquitous element that circulates in different forms in the atmosphere. It is also known as "king of poisons and poisons of kings". Sometimes, local geological formations and human activities lead to higher arsenic concentrations. Arsenic is the 20th most ample element present in the earth's crust (Singh et al. **2004**).

Arsenic is present in the environment in two ways either naturally or by anthropogenic activities. Naturally, arsenic can be obtained from the volcanic eruption, wild and fires, geothermal activities and weathering of rock (Kavcar et al. **2009**; Yazdani et al. **2016**). Anthropogenic activities which causes arsenic contamination are smelting, mining, wood preservatives, burning of coal, glass industry, pesticides, incinerators, municipal waste, manufacturing of semi-conductors, insecticides, industrial wastes, and herbicides (Mandal et al. **2002**; Ali et al. **2019**; Chowdhury et al. **2011**). Arsenic is found in two forms, inorganic and organic whereas inorganic is more toxic than organic arsenic. Arsenic when present by the accumulation in the food chain it can be lethal for human beings. There are various diseases associated with arsenic for example skin, bladder, lung, kidney, lung cancer, reproductive disorders, neurological disorders, cardiovascular issues, high blood pressure, diabetes and many others (Basu et al. **2005**; Rahman et al. **1999**; Wang et al. **2011**). Figure 1 shows the schematic diagram of arsenic contamination sources.

Thus, there is an urgency to innovate a novel product to remove arsenic from water. To address this need, researchers worldwide are working to develop constructive, cost-effective and productive technologies for the removal of organic and inorganic arsenic from water. Significant advances have been made in material sciences—specifically, in material synthesis—to meet objectives that were once impossible. The establishment of many conventional adsorbents: such as titanium, aluminum, and iron have been used for arsenic removal. This application of nanotechnology using low-cost materials to cope up with environmental degradation processes and will enhance the knowledge of environmental protection agencies, government, and industries while protecting water bodies and preventing agricultural runoff. Successful harnessing of nanotechnology to address arsenic will ultimately reduce water pollution generated by human activities and aquatic life.

Nanotechnology involves the manipulation of various materials on the atomic level; on this scale, the chemical and physical properties of numerous organic and inorganic species can be altered (Benelmekki **2015**). The study and manipulation of a material on a nanoscale permit the scientific community to contribute and synthesize different materials to obtain specific properties and characteristics. This enables the achievement of a wide range of technological advancements in the fields of environment, optics, health, electronics, and so on (Pradeep **2003**). Nanomaterials have also been used widely in the environmental monitoring of water (Su et al. **2012**). An assortment of arsenic degradation advancements exist and broad reviews of these procedures have been published (Ali et al. **2004**; Ali **2010**). The water treatment technology developed here in will have considerable economic benefits achieved by reducing the cost of water analysis and treatment processes. Metal oxides promise incredible guarantee because they have a higher affinity and selectivity for heavy metal ions such as As (III) and As (V) (Ray et al. **2015**; Lata et al. **2016**).

Arsenic is ever-present in the environment and its toxicity makes it lethal to all living beings. It has become a sign of danger for all over the world, especially for Asian countries. Communities in Pakistan are unable to approach the high quality of drinking water. By consuming contaminated water, people face different skin diseases as arsenic is carcinogenic too.

Arsenic toxicity in water resources has become a serious public health concern in Pakistan. The problem is especially prevalent in Sindh, where about 36% of the population is at risk for arsenic contamination because it is present in surface and groundwater above the limits of the World Health Organization (WHO). High arsenic contaminated (> 50 mg L^{-1}) groundwater has been reported in various parts of the world (Bhattacharya et al. **2002**). It is generally accepted that inorganic compounds like arsenite [As^{3+}] and arsenate [As^{5+}] are the predominant forms of As in most environments, though organic forms (arsenobetaine and arsenocholine) could also be present (Andrianisa et al. **2008**). This research will provide the best remedial solution for removal of arsenic contamination for local community of Sindh, Province. The poverty of the rural Sindh is obvious from the fact that this area housing almost half of the province's population contributes only 30% of the Sindh's GDP. In rural Sindh, mostly poor people are the most affected population from water impairment due to their limited means of livelihoods and low-income levels. Besides low awareness of water quality related health issues, these people cannot afford

buying high quality drinking water and have to rely on whatever is available to them. In addition, when they get sick, they cannot meet the expenses of medical treatment and hospitals. The advanced treatment technology in this project is cost effective and hence affordable for the poor people of the rural Sindh. Iron oxide nanoparticles, due to their high electrical conductivity, chemical stability, biocompatibility, and magnetic behavior they have getting attention. It is reported several times that the characteristics vary with the size, crystal phase, and shape. Magnetite nanoparticles are fabricated in various methods, but most stable and ecofriendly method is the co-precipitation to be the most frequent for magnetite nanoparticles.

In this research, we used magnetite iron oxide nanoparticles as they are non-hazardous and possess economic advantages over other nanoparticles used commonly. L-Cysteine is used as the capping agent as it plays a long-term stability role in magnetite NPs. Amino acid as a surfactant agent; also they are less harmful and currently used as reagents in many studies. After the literature reviewed, we have found that a lot of work has been done on the Iron oxide nanoparticles all over the world even in Pakistan but none use L-Cysteine as the stabilizing/reducing agent, which is a greener chemical. This chemical enhances the removal efficiency of arsenic from the water. From the above-mentioned literature, it is clear that many studies are going on the removal, degradation, and adsorption of arsenic and other contaminants from the water. Many researchers have worked on the elimination of arsenic from the water in many ways but no study was found on the removal of arsenic using L-Cysteine capped iron oxide nanoparticles. Herein, we report the simple and greener method for the synthesis of iron oxide nanoparticles and their efficient catalytic degradation ability towards arsenic from water source.

2 Materials And Methods

2.1 Chemicals and Reagents

Precursors used in this study are ferric chloride hexahydrate ($FeCl_3 \cdot 6H_2O$), ferrous chloride tetrahydrate ($FeCl_2 \cdot 4H_2O$). Sodium hydroxide (NaOH) is used as a reducing agent while L-Cysteine is used as a capping agent and was purchased by Daejung Chemicals & Materials Co. Ltd. Nitric acid of 70% was used to dissolve L-Cysteine.

2.2 Preparation of stock solution

The arsenic stock solution was prepared by standard solution of 1000 ppm (1 million ppb) purchased from VWR Chemicals, USA. It was then diluted in the desired concentration for the experiment. All the preparation was done in the volumetric flask to avoid errors. The pH of Deionized water was checked before the dilution and five different concentrations were made by diluting to 10 ppm (1 ppm, 0.5 ppm, 0.1 ppm, 0.05 ppm and 0.001 ppm).

2.3 Synthesis of iron oxide (Fe_3O_4) nanoparticles in aqueous solution

The aqueous Iron oxide solution was prepared by the salts i-e $FeCl_3$. $6H_2O$ and $FeCL_2$.$4H_2O$ with a concentration of 0.2 M and 0.1 M, respectively. Ferric chloride hexahydrate was diluted in 100 ml of deionized water and kept on a magnetic stirrer hot plate for 10 minutes. After the mixing, ferrous chloride tetrahydrate was diluted in 100 ml of DI and mixed to the solution at a magnetic stirrer for 30 minutes. On the other hand, L-Cysteine of 0.1 M was prepared using nitric acid and then added to the solution for the prevention of agglomeration. After 10 minutes, Sodium hydroxide (NaOH) of 0.5 M was added gradually to maintain the pH from 9–12 and allowed the mixture for vigorous mixing for 4–5 hours until the precipitates formed. The denser liquid present at the bottom due to magnetic properties was collected and passed through the filter. It was rinsed three times with ethanol and DI to remove impurities. In the end, it was kept in an oven for 4 hours at 60°C and collected for experimental purposes.

2.4 Site selection

District Larkana of Sindh province is situated by the side of the Indus River and covers five tehsils, Ratodero, Warah, Miro Khan, Dokri and Larkana with a total land area of 7423 km^2. It is the fourth largest city of Sindh with a population of 1.5 million (CENSUS 2017). The residents of Larkana use groundwater for drinking purposes. (Ali et al. 2019), investigated the cause of arsenic enrichment in the water of Larkana in 2019 and concluded that the level of arsenic is from 2 ppb to 318 ppb in the drinking water, which is above the level of WHO. This research creates enthusiasm to collect water from the sachal colony, Larkana and to test the synthesized material. Figure 2a, there is a map, which showed the levels of arsenic present in water and in Fig. 2b, shows the area selected for the collection of water. The cause of arsenic enrichment in Larkana's water is vertical mixing with return irrigation water.

2.5 Water sampling frequency and sampling protocols

In our experimental study, we collected a small portion of water randomly from different parts of Sachal Colony, Larkana. The number of samples was eight. The volume per sample was 900 ml so that they can be tested in triplicates. They were collected in a 1-liter bottle and we did onsite water quality testing also. The basic purpose of water sampling and testing was to check the change occurred in previous studies until now.

2.6 Sample collection and transportation

The samples were collected in the autoclaved plastic bottles of 1 liter from the Sachal Colony, District Larkana and were placed in ice-box for the transportation to US-Pakistan Center for advanced studies in water, advanced water and waste water quality control laboratory, MUET, Jamshoro. The bottles were filled until 900 ml and capped properly so that the effect of evaporation can be reduced. They were preserved in hydrochloric acid because samples having metals can be perfectly preserved with the help of acid. They were placed in the refrigerator to maintain the temperature and for further experiments.

2.7 Water sample preparation for analysis

Samples were prepared with different dosage of L-Cysteine functionalized iron oxide nanoparticles and concentration of arsenic varies. The real water samples were also kept with different dosages for 1 hour on the flask shaker so that the particles can easily be mixed. They were poured in 20ml glass bottles for the analysis of ICP-MS. The model no of flask shaker is 1220K73 and Mfr. No is 401000-2. The model no of the orbital shaker used for this study was 1165U07.

2.8 Characterization techniques

The prepared L-Cysteine derived iron oxide nanoparticles were characterized by using different characterization technique's such as UV-Visible Spectroscopy (UV-Vis) Shimadzu, Energy Dispersive Spectroscopy of Bruker-x-flash (6060, USA), Zeta Potential Analyzer Malvern instruments ltd. (serial no. MAL- 1, 135,362), Transmission Electron Microscopy (TEM) (Philips CM12, FEI Ltd., UK), X-ray Diffraction (XRD) Horiba, and Fourier Transform Infrared Spectroscopy (FT-IR) Thermo Scientific and Inductively Coupled Plasma Mass Spectroscopy (ICP-MS) model NexION 350Q, Perkin Elmer.

3.9 Application study by inductively coupled plasma mass spectroscopy (ICP-MS)

For this study, inductively coupled plasma mass spectroscopy (ICP-MS), model NexION 350Q by Perkin Elmer was used for the analysis as shown in Fig. 3. ICP-MS reduces interferences and background, minimizes maintenance requirements, optimizes signal stability and it generates better results. It offers detection limits for calcium, selenium, iron, arsenic, chromium, potassium, magnesium and vanadium. The suited application of this model is the simple analyses with no requirement of interference and includes routine geochemical analysis.

3 Results And Discussion

3.1 Calibration curve of arsenic

ICP-MS demonstrates ion when influencing electron multiplier especially on the dynode and it behaves as a detector. When the ions influence the dynode, there is a release of electrons and a measurable pulse is generated. Then the built-in software of ICP-MS relates the intensities and makes the calibration curve. In this study, the calibration curve was prepared for the analysis of ICP-MS to know the exact concentration of arsenic present in the solution. Linear line shows the value of R^2 at 0.999 as shown in Fig. 4.

3.2 Characterization of adsorbent

3.2.1 UV- Visible Spectroscopy (UV-Vis)

The absorption range of the incorporated L-cysteine derived iron oxide nanoparticle, were seen in the middle of the scope of 300-700nm wavelength. The colloidal Fe_3O_4 NPs were gotten and scattered in de-

ionized water after the sonication process (25 minutes). Reported study, shows the fabricated NPs were in the range 375 and 650 nm

(Chaki et al. **2015**). In our study, the peak appeared at 394 nm of the synthesized iron oxide NPs as shown in Fig. 5.

3.2.2 Transmission Electron Microscopy (TEM)

In material sciences, TEM is used as a powerful tool for a high-resolution image. A beam of high energy of electrons moves directly towards the sample of 0.2nm. This technology investigated the shape, size and used as chemical analysis. The crystallinity, spherical morphology and size of the synthesized L-cysteine capped iron oxide NPs were analyzed as shown in Fig. 6a. The size appeared were in the range of 5-35nm and mostly were of 15nm as shown in Fig. 6b. They showed to be in a spherical shape as shown in Fig. 6a. ImageJ software was used to analyze the sizes of the particles. (Yew et al. **2016**), observed that most particles were ranging 10-18nm.

3.2.3 Zeta Potential Analyzer

Zeta Potential is used to know the net surface charge of the nanoparticles and is a physical property. It also confirmed the stability of the nanoparticles concerning the surface potential charge. The stability of particles can be obtained at the most optimum line between the stable and unstable nanoparticles, which are generally expressed in the range of + 30mV to -30mV. This study showed that L-cysteine capped iron oxide NPs were stable with a value of – 29.7mV as shown in Fig. 7. (Madhavi et al. **2013**), showed that the nanoparticles were stable and contained a highly negative charge.

3.2.4 Electron Dispersion Spectrum (EDS)

EDS technique describes more about the chemical composition of the material, it also tells about the purity of the material. The spectrum at 1.73KeV at spots was examined. There were two maximum peaks of the spectrum were acquired as shown in Fig. 8. The quantitative analysis of this study revealed that there were more 68.17% weight atoms of iron are present in the synthesized Fe_3O_4 nanoparticles as shown in Fig. 8. (Radwa et al. **2016**), showed that the L-cysteine is used as the stabilizing agent.

3.2.5 X-Ray Diffraction Spectroscopy

X-ray diffraction was used to determine the phase purity and the crystalline structure of the nanoparticles. The advantage of using this technique is that does not harm or damage the material and it provided results efficiently. The X-ray diffraction patters of synthesized L-cysteine capped nanoparticles showed

the existence of the crystalline structure of the nanoparticles as shown in Fig. 9. The XRD peaks were matched with reported literature (Khalafi-Nezhad et al. **2015**; Panhwar et al. **2019**). All peaks are matched with the characteristics of magnetite material and it proposed the core-shell structure of synthesized iron oxide NPs as shown in Fig. 9.

3.2.6 Fourier Transform Infrared Spectroscopy (FT-IR)

FT-IR is a useful tool for characterizing the particles. It tells more about the capping and reduction occurring within the synthesized material. As shown in Fig. 10, the different FTIR peaks were observed. A peak at 1727cm^{-1} shows the presence of acidic carbonyl groups (C = O). A peak at 1083cm^{-1} is due to carboxyethylsilanetriol (CES) (C-O) group (Sh**arifi** et al. **2013**). A peak at 1337cm^{-1} shows the adsorption band due to CH_2 groups (bending variations). A peak at 1540cm^{-1} bending vibration is present (Ma et al. **2016**). A peak at 2284cm^{-1} shows the presence of amide groups and COO^{-1}.

3.3 Mechanism

Arsenic creates many acute and chronic diseases in the human body. Many various technologies have been used in the past for the removal of arsenic from the water. Iron oxide adsorbents are dominant in the field of adsorption of arsenic because of its capacity. The adsorption of arsenic is mainly dependent on the quantity of iron present because iron adsorbent have the maximum ability to adsorb arsenic from the water. In our study, the L-cysteine was used as a stabilizing agent to prepare the desired particles. When the particles were fabricated it was then reacted with arsenic so that it can adsorb. After the reaction, the arsenic is reduced due to nanoparticles present in the solution. The following reaction shows how the arsenic was been adsorbed on the iron oxide nanoparticles.

3.4 Effect of adsorbent dose

The adsorption of arsenic onto the L-Cysteine functionalized Iron oxide Nanoparticles are influenced by adsorbent dose. The effect of the dose of NPs on arsenic is shown in Fig. 11.

The removal percentage caused by a dose of Iron NPs of equilibrium concentrations of arsenic increases by increasing the adsorbent dose from 30 mg to 80 mg. The removal of arsenic from the aqueous solution increased from 95.4–99.8%. The highest removal efficiency was achieved when the maximum dose of adsorbent was added, due to the availability of maximum vacant spaces present on the surface of the adsorbent. The quantity of the adsorbent used in an experiment is directly proportional to the number of sites available for adsorption (Elaigwu et al. **2014**).

3.5 Effect of pH

The effect of pH on the adsorption is shown in Fig. 12. It is seen that the range from 5.5 to 7.5, the adsorption is higher as compared to others. At pH 6, there is maximum adsorption.

The percent of removal of arsenic increases from 16–99.1%, as the pH increases from 4 to 8. The low adsorption rate at pH 4, which indicates that solution, becomes H^+ charged and that repels the molecules of the adsorbent. Moreover, as pH rises from 4 to 8 H^+ ions (positive) are replaced with OH^- (negative) ions which makes arsenic molecules to attach onto the surface of the adsorbent. It is reported in the literature that the arsenic becomes unstable at higher pH (Takeno **2005**) whereas (Irem et al. **2017**), reported that the maximum adsorption of arsenic was on pH 6.

3.6 Effect of concentration

The effect of various concentrations on adsorption was studied using a range of arsenic concentrations from 0.01 ppm – 1 ppm (10 ppb – 1000ppb) at a fixed adsorbent dose of 80 mg, using an orbital shaker speed of 150 rpm at room temperature. The batch study **is** shown in Fig. 13. The results depict that there was a maximum removal in the lowest concentration at 0.01 ppm (10 ppb) was 99.85% and the minimum removal was observed in the highest concentration at 1 ppm (1000 ppb) was 94.45% as shown in Fig. 14. Even at 0.5ppm (500ppb), the removal efficiency was 98.9% after one hour.

3.7 Equilibrium isotherms

For to understand the functioning of adsorbing molecule and adsorbent for the optimization process design (Lakshmi et al. **2009**). From the experimental data, the values were put into two isotherm models. Isotherm parameters for each model was obtained from intercept and slope of model equation.

3.7.1 Langmuir Isotherm Model

The Langmuir isotherm model believes that the adsorption happens at certain equivalent destinations inside the adsorbent. The monolayer adsorption venture is shown as (Langmuir **1918**).

In Langmuir model, the adsorption

$$C_e/q_e = 1/Q_{max} * K_L + C_e/Q_{max} \text{ ———————} (3)$$

The values Q_{max} and K_L can be calculated from the slope and the intercept of the linear plot shown in Fig. 14. The value and constant of R^2 from the equilibrium data shown in Table 2.

Table 1
Water sampling frequency.

Point of Sampling	No: of samples	Type of analysis	Volume	Onsite testing	Control Monitoring	Frequency
Handpumps/ Drilling well/ tap water	8	Physical and Chemical	300ml in triplicates	Yes (pH, EC, TDS, Temperature, Turbidity and Arsenic)	Sampling	Random

Table 2
Isotherms study of removal arsenic by ICP-MS.

Isotherms					
Langmuir			Freundlich		
q_{max}	B	R^2	N	k_f	R^2
1.96	145.4	0.99	2.73	0.367	0.7551

The important characteristic of the Langmuir isotherm can be demonstrated as the dimensionless constant separation factor R_L which is shown by this equation

The significant normal for the Langmuir isotherm can be exhibited as the dimensionless constant factor RL which is appeared by this condition (Hall et al. **1966**).

$R_{L} = 1/(K_L+C_o)$ ——— (4)

In the Freundlich isotherm, surface adsorption occurs in multilayer or heterogeneous (Fawzy et al. **2016**) [46]. The Freundlich equation is follows as (Freundlich **1906**).

$\log q_e = \log K_F + 1/n *(\log C_e)$ ———— (5)

The values of K_F and 1/n will be obtained from the linear plot of log q_e versus log C_e shown in Fig. 15. The isotherm parameters and R^2 value are presented in Table 4.1.

In this isotherm study, it was well concluded that the Langmuir isotherm fitted the best for the synthesized nanoparticles as shown in Fig. 14. The maximum adsorption capacity was calculated to be 1.96 mg/g. The parameters of both the models, Langmuir and Freundlich are mentioned in Table 2. The values are being checked by different researches and they used three isotherm models (Monárrez-Cordero et al. **2016**; Rahdar et al. **2019**), whereas this study performed only two isotherm models.

3.8 Kinetic study

For the determination of efficiency of adsorbent in relation of solute consuming rate which can be described by adsorption kinetics. Therefore, the experimental data was shown through pseudo first-order, pseudo second-order to describe the mass transfer process.

3.8.1 Pseudo-first-order model

The Pseudo first-order equation (Lagergren 1898) can be expressed as:

$\ln (q_e - q_t) = \ln q_e - k_{1*} t$ ——— (6)

The value of k_1 and qe can be calculated from slope and intercept by plotting graph between, ln ($q_e - q_t$) versus t as shown in Fig. 16, and the values of constants are presented in Table 3.

Table 3
Kinetic study of removal arsenic by ICP-MS.

Kinetics					
Pseudo 1st Order kinetic			Pseudo 2nd Order kinetic		
k_1	q_e	R^2	k_2	q_e	R^2
0.034	14.2	0.12	0.476	1.47	0.99

3.8.2. Pseudo-second-order model

The pseudo second-order model can be expressed as (Ho et al. **1999**);

$t/q_t = k_2 q^2_e + t/q_e$ ---------- (7)

k_2 = a second-order rate equation constant and can be obtained by plotting the graph t/q_e versus t, shown in Fig. 17, and the calculated values of constants are shown in Table 3.

In the current study, the kinetics of arsenic removal was studied to find and to know the adsorption capacity and adsorption behavior. Adsorption increased with the passage of time as there are vacant spaces available on the adsorbent but after the equilibrium achieved the adsorption starts to decrease and become resistant as the vacant site are occupied. This work followed Pseudo 2nd order and confirms the chemical adsorption as shown in Fig. 18, whereas, Pseudo 1st order confirms physical adsorption. (Rahdar et al. **2019**) also performed the datasets into the kinetic study i.e., two models. In this study, Pseudo 2nd order fitted the best. The values for both kinetic orders are mentioned in Table 3.

3.9 Testing of real water samples

As discussed in methodology part, three areas were select for the site selection, sample preparation and analysis on ICP-MS of real water. The basic physical and chemical parameters of water samples are shown in Table 4.

Table 4
Physical and chemical parameters of water samples.

\S1/**/ample 8/ID	Turbidity	pH	Electrical Conductivity	TDS
1	0.15	7.1	507.6	329.94
2	0.45	6.2	555.3	360.94
3	0.23	7.43	620.1	403.06
4	1.2	7.56	486.8	316.42
5	0.67	7.34	532.7	346.25
6	0.43	7.12	489.9	318.43
7	0	7.41	615.6	400.14
8	0.21	6.97	634.5	412.425

After testing the basic parameters, we then tested arsenic presence by the arsenic kit. It confirmed the arsenic presence in the water and after then the samples were collected. Those samples were than tested on ICP-MS for further confirmation and to know the initial reading, after knowing the initial arsenic level 80mg of iron oxide NPs, were added and kept on stirrer for 30 and 60 min as shown in Fig. 18.

Fluoride was also tested through spectrophotometer (DR-1900) but none of the sample had more fluoride than the permissible limit. The permissible limit of fluoride by WHO was reported at 1.5 ppm. Table 5, it can be seen that the maximum removal after 30 minutes was 77.3% and when it kept for 60 minutes, the maximum adsorbed efficiency was 81.09%. Table 6 shows the comparison data of the reported and this present study.

Table 5
Removal efficiency of arsenic at 30 and 60 minutes.

Sample ID	Initial concentration (ppb)	Final Concentration (ppb), 30 mints (80mg NPs)	Percentage (%)	Final Concentration (ppb), 60 mints (80 mg NPs)	Percentage (%)
1	55.6	16.3	70.6	14.1	74.64
2	62.1	20.4	67.1	16.2	73.91
3	43.2	13.4	68.98	11.3	73.84
4	28.2	6.4	77.3	5.5	80.4
5	59.3	19.8	66.61	16.1	72.8
6	45.8	15.2	65.06	13.1	71.39
7	53.4	17.1	67.97	15.2	71.53
8	32.8	8.2	75	6.2	81.09

Table 6
Comparison data with reported studies.

S No:	Adsorbent	Adsorption Capacity (mg g^{-1})	Reference
1	Fe_2O_4	0.2	Turk, Alp and Devici (2010)
2	CuO nanoparticles	1.1	Pena et al. (2005)
3	Cross linked polyethylenimine	1.4	Saad, Cukrowska and Tutu (2013)
4	Wood Shavings at 250C	0.001	Lima et al. (2015)
5	Fe_2O_4 Nanomaterial	1.25	Tian et al. (2011)
6	Iron Oxide coated Sand	0.029	Thirunavukkarasu, Viraraghavan and Subramanian (2003)
7	Iron Oxide coated Cement	0.69	Kundu and Gupta (2007)
8	Chitosan/PVA Nanofibers (CP)	1.68	Chauhan, Dwivedi, and Sankararamakrishnan, (2014)
9	Oak-Wood Biochar	3.16	Niazi et al. (2018)
10	Perilla Leaf Biochar	4.71	Niazi et al. (2018)
11	L-Cysteine Derived Iron Oxide Nanoparticles	1.96	Present Study

Conclusions

In this study, Iron oxide nanoparticles were synthesized using a greener chemical named as L-Cysteine. It is protein-rich, comes in amino acid and is sold commercially as a dietary supplement. Moreover, synthesized L-Cysteine capped iron oxide nanoparticles were tested for the removal of arsenic from synthetic as well as real water samples. The synthesized iron oxide nanoparticles were characterized by different analytical techniques such as transmission electron microscope (TEM), was confirmed the smallest particle size in the range of 5–30 nm, ultraviolet-visible spectroscopy (UV-Vis) spectrum confirmed the formation with wavelength occurred at 394 nm, X-ray Diffraction (XRD) patterns showed the presence of crystalline structure, energy dispersive spectroscopy (EDS) also proved the highest elemental percent of iron as compared to other element, zeta potential analyzer confirmed the net surface potential charge and stability of the nanoparticles having − 29.7 mV value and Fourier transform infrared spectroscopy (FTIR) technique determine the functionality between the interaction of metal salts with reducing/stabilizing agent. After the characterization, it is proved that the synthesized particles have the higher surface area and they were spherical. The effect of synthesized L-Cysteine capped iron oxide nanoparticles dose, concentration and pH were determined. It was observed due to the higher surface

area present; the arsenic was adsorbed rapidly until the equilibrium stage was achieved. The adsorption capacity of arsenic on the prepared iron oxide nanoparticles was 1.96 mg/g and 80 mg was the maximum dose used. The adsorption dataset best fits in the Langmuir model and does not follow the Freundlich model. Hence, the adsorption was in monolayer. From the kinetic study, it can be concluded that this adsorption obeyed the pseudo-second-order model. This study showed that the fabricated nano-particles were never used for the removal of arsenic in any study and proved to be highly efficient. They are easy to make and do not require an extensive workforce. By checking its practical application on real water samples, it can be concluded that its efficiency is better and can be further tested.

Declarations

Conflict of interests

Authors have declared that there is no conflict of interests

Author's contribution

SSH, ZA, MYT and SP conceived of the presented idea. SSZ carried out the experiment. SSZ wrote the manuscript with guidance from SSH, ZA, MYT and SP. All authors discussed the results and contributed to the final manuscript.

Acknowledgments

The authors would like to thank US.-Pakistan Centre for Advanced Studies in Water (USPCAS-W), Mehran University of Engineering and Technology (MUET), Jamshoro, Sindh 76062, Pakistan for providing a pleasant environment for research work and USAID for providing the financial support to carry out this research work.

References

1. Ali, I. (2010). The quest for active carbon adsorbent substitutes: inexpensive adsorbents for toxic metal ions removal from wastewater. Separation & Purification Reviews, 39, 95–171.
2. Ali, I. and Jain, C.K. (2004). Advances in arsenic speciation techniques. International Journal of Environmental Analytical Chemistry, 84, 947–964.
3. Ali, W., Mushtaq, N., Javed, T., Zhang, H., Ali, K., Rasool, A. and Farooqi, A. (2019). Vertical mixing with return irrigation water the cause of arsenic enrichment in groundwater of district Larkana Sindh, Pakistan. Environmental Pollution, 245, 77–88.
4. Ali, W., Mushtaq, N., Javed, T., Zhang, H., Ali, K., Rasool, A. and Farooqi, A. (2019). Vertical mixing with return irrigation water the cause of arsenic enrichment in groundwater of district Larkana Sindh, Pakistan. Environmental Pollution, 245, 77–88.

5. Andrianisa, H. A., Ito, A., Sasaki, A., Aizawa, J., Umita, T. (2008). Biotransformation of arsenic species by activated sludge and removal of bio-oxidised arsenate from wastewater by coagulation with ferric chloride. Water Research, 42, 4809-17.
6. Ashour, R. M., Abdel-Magied, A. F., Abdel-khalek, A. A., Helaly O. S., Ali. M. M. (2016). Preparation and characterization of magnetic iron oxide nanoparticles functionalized by l-cysteine: Adsorption and desorption behavior for rare earth metal ions. Journal of Environmental Chemical Engineering, 4, 3114–3121.
7. Basu, A., Som, A., Ghoshal, S., Mondal, L., Chaubey, R. C., Bhilwade, H. N., Rahman, M. M., Giri, A. K. (2005). Assessment of DNA damage in peripheral blood lymphocytes of individuals susceptible to arsenic induced toxicity in West Bengal, India. Toxicology Letters. 159, 100–112.
8. Benelmekki, M. (2015). Designing hybrid nanoparticles. Morgan & Claypool Publishers.
9. Bhattacharya, P., Jacks, G., Ahmed, K.M., Routh, J. and Khan, A.A. (2002). Arsenic in groundwater of the Bengal Delta Plain aquifers in Bangladesh. Bulletin Environmental Contamination and Toxicology, 69, 538–545.
10. Chaki, S.H., Malek, T.J., Chaudhary, M.D., Tailor, J.P. and Deshpande, M.P. (2015). Magnetite Fe_3O_4 nanoparticles synthesis by wet chemical reduction and their characterization. Advances in Natural Sciences: Nanoscience and Nanotechnology, 6, 035009.
11. Choong, T. S.Y., Chuah, T. G., Robiah, Y., Koay, F. L. G., Azni, I. (2007). Arsenic toxicity, health hazards and removal techniques from water: an overview. Desalination 217, 139–166.
12. Chowdhury, M. R. I., Mulligan, C.N. (2011). Biosorption of arsenic from contaminated water by anaerobic biomass. Journal of Hazardous Materials, 190, 486 – 92.
13. Elaigwu, S.E., Rocher, V., Kyriakou, G., Greenway, G.M. (2014). Removal of Pb^{2+} and Cd^{2+} from aqueous solution using chars from pyrolysis and microwave-assisted hydrothermal carbonization of Prosopis africana shell. Journal of Industrial and Engineering Chemistry, 20, 3467–3473.
14. Emenike, C. P., Tenebe, I. T., Omole, D. O., Ngene, B. U., Oniemayin, B. I., Maxwell, O., Onoka, B. I. (2017a). Accessing safe drinking water in sub-Saharan Africa: Issues and challenges in south-west Nigeria. Sustainable Cities and Society, 30, 263–272.
15. Fawzy, M., Nasr, M., Helmi, S., Nagy, H. (2016). Experimental and theoretical approaches for Cd(II) biosorption from aqueous solution using Oryza sativa biomass. International Journal of Phytoremediation, 18(11):1096–1103.
16. Freundlich, H.M.F. (1906). Over the adsorption in solution. The Journal of Physical Chemistry, 57, 1100–1107.
17. Gul, M., Mashhadi, A. F., Iqbal, Z., Qureshi, T. I. (2020). Monitoring of arsenic in drinking water of high schools and assessment of carcinogenic health risk in Multan, Pakistan. Human and Ecological Risk Assessment: An International Journal, 26, 2129 – 214.
18. Hall, K.R., Eagleton, L.C., Acrivos, A. and Vermeulen, T. (1966). Pore-and solid-diffusion kinetics in fixed-bed adsorption under constant-pattern conditions. Industrial & Engineering Chemistry Fundamentals, 5, 212–223.

19. Hassan, S. S., Sirajuddin, Solangi, A. R., Kazi, T. G., Kalhoro, M. S., Junejo, Y., Tagar, Z. A., Kalwar, N. H. (2012). Nafion stabilized ibuprofen–gold nanostructures modified screen printed electrode as arsenic(III) sensor. Journal of Electroanalytical Chemistry, 682, 77–82.
20. Ho, Y.S. and McKay, G. (1999). Comparative sorption kinetic studies of dye and aromatic compounds onto fly ash. Journal of Environmental Science and Health A, 34, 1179–1204.
21. Irem, S., Islam, E., Mahmood Khan, Q., Anwar ul Haq, M. and Jamal Hashmat, A. (2017). Adsorption of arsenic from drinking water using natural orange waste: kinetics and fluidized bed column studies. Water Supply, 17,1149–1159.
22. Kavcar, P., Sofuoglu, A., Sofuoglu, S. C. (2009). A health risk assessment for exposure to trace metals via drinking water ingestion pathway. International Journal of Hygiene Environmental Health, 212, 216–227.
23. Khalafi-Nezhad, A., Nourisefat, M. and Panahi, F. (2015). L-Cysteine functionalized magnetic nanoparticles (LCMNP): a novel magnetically separable organocatalyst for one-pot synthesis of 2-amino-4 H-chromene-3-carbonitriles in water. Organic and Biomolecular Chemistry, 13, 7772–7779.
24. Khan, S., Shahnaz, M., Jehan, N., Rehman, S., Shah, M. T., Din, I. (2013). Drinking water quality and human health risk in Charsadda District, Pakistan. Journal of Cleaner Production, 60, 93–101.
25. Lagergren. S. (1898). Zur theorie der sogenannten adsorption geloester stoffe Veternskapsakad. Handl., 24:1–39.
26. Lakshmi, U.R., Srivastava, V.C., Mall, I.D., Lataye, D.H. (2009). Rice husk ash asan effective adsorbent: evaluation of adsorptive characteristics for Indigo Carminedye. Journal of Environmental Management, 90:710e720.
27. Langmuir, I. (1918). The adsorption of gases on plane surfaces of glass, mica and platinum. Journal of American Chemical Society, 40, 1361–1403.
28. Lata, S. and Samadder, S.R. (2016). Removal of arsenic from water using nano adsorbents and challenges: a review. Journal of Environmental Management, 166, 387–406.
29. Li, P. Y., Qian, H., Howard, K. W. F., Wu, J. H., Lyu, X. S. (2014a). Anthropogenic pollution and variability of manganese in alluvial sediments of the Yellow River, Ningxia, Northwest China. Environmental Monitoring and Assessment, 186, 1385–1398.
30. Li, P. Y., Qian, H., Wu, J. H., Chen, J., Zhang, Y. Q., & Zhang, H. B. (2014b). Occurrence and hydrogeochemistry of fluoride in shallow alluvial aquifer of Weihe River, China. Environmental Earth Sciences, 71, 3133–3145.
31. Ma, X., Guo, Q., Xie, Y. and Ma, H. (2016). Green chemistry for the preparation of L-cysteine functionalized silver nanoflowers. Chemical Physics Letters, 652, 148–151.
32. Madhavi, V., Prasad, T.N.V.K.V. and Madhavi, G. (2013). Synthesis and spectral characterization of iron based micro and nanoparticles. Iranian Journal of Energy and Environment, 4, 385–390.
33. Malassa, H., Hadidoun, M., Al-Khatib, M., Al-Rimawi, F., Al-Qutob, M. (2014). Assessment of groundwater pollution with heavy metals in North West Bank/Palestine by ICP-MS. Journal of Environmental Protection, 05, 54–59.

34. Mandal, B.K. and Suzuki, K.T. (2002). Arsenic round the world: a review. Talanta, 58, 201–235.
35. Monárrez-Cordero, B.E., Amézaga-Madrid, P., Leyva-Porras, C.C., Pizá-Ruiz, P. and Miki-Yoshida, M. (2016). Study of the Adsorption of Arsenic (III and V) by Magnetite Nanoparticles Synthetized via AACVD. Materials Research, 19, 103–112.
36. Mudhoo, A., Sharma, S. K., Garg, V. K., Tseng, C. H. (2011). Arsenic: an overview of applications, health, and environmental concerns and removal processes. Critical Reviews in Environmental Science and Technology. 41, 1–86.
37. Mushtaq, N., Younas, A., Mashiatullah, A., Javed, T., Ahmad, A., Farooqi, A. (2018). Hydrogeochemical and isotopic evaluation of groundwater with elevated arsenic in alkaline aquifers in Eastern Punjab, Pakistan. Chemosphere, 200, 576–586.
38. Nickson, R. T., McArthur, J.M., Shrestha, B., Kyaw-Myint, T.O., Lowry, D. (2005). Arsenic and other drinking water quality issues, Muzaffargarh District, Pakistan. Appl Geochem. 20, 55–68.
39. Panhwar, S., Hassan, S.S., Mahar, R.B., Carlson, K. and Talpur, M.Y. (2019). Highly Sensitive and Selective Electrochemical Sensor for Detection of Escherichia coli by Using L-Cysteine Functionalized Iron Nanoparticles. Journal of Electrochemical Society, 166, B227-B235.
40. Pradeep, T. (2003). A textbook of nanoscience and nanotechnology. Tata McGraw-Hill Education.
41. Rahdar, S., Rahdar, A., Khodadadi, M., Ahmadi, S. (2019). Error analysis of adsorption isotherm models for penicillin G onto magnesium oxide nanoparticles. Applied Water Science, 9, 190.
42. Rahman, M., Tondel, M., Chowdhury, A. I., Axelson, O. (1999). Relations between exposure to arsenic, skin lesions, and glucosuria. Occupational and Environmental Medicine, 56, 277 – 81.
43. Ray, P.Z. and Shipley, H.J. (2015). Inorganic nano-adsorbents for the removal of heavy metals and arsenic: a review. RSC Advances, 5, 29885–29907.
44. Sharifi, S., Daghighi, S., Motazacker, M.M., Badlou, B., Sanjabi, B., Akbarkhanzadeh, A., Rowshani, A.T., Laurent, S., Peppelenbosch, M.P. and Rezaee, F. (2013). Superparamagnetic iron oxide nanoparticles alter expression of obesity and T2D-associated risk genes in human adipocytes. Scientific Reports, 3, 2173.
45. Singh, T. S., Pant, K. K. (2004). Equilibrium, kinetics and thermodynamic studies for adsorption of As (III) on activated alumina. Separation and Purification Technology, 36, 139–147.
46. Su, S., Wu, W., Gao, J., Lu, J. and Fan, C. (2012). Nanomaterials-based sensors for applications in environmental monitoring. Journal of Materials Chemistry, 22, 18101–18110.
47. Takeno, N. (2005). Geological Survey of Japan, Atlas of Eh-pH Diagrams, Geological Survey of Japan Open File Report No. 419: National Institute of Advanced Industrial Science and Technology Research Center for Deep Geological Environments.
48. Wang, Z., Chai, L., Wang, Y., Yang, Z., Wang, H., Wu, X. (2011). Potential health risk of arsenic and cadmium in groundwater near Xiangjiang River, China: a case study for risk assessment and management of toxic substances. Environmental Monitoring and Assessment, 175, 167–173.

49. Xing, L., Guo, H., Zhan, Y. (2013). Groundwater hydrochemical characteristics and processes along flow paths in the North China Plain. Journal of Asian Earth Sciences. 70–71, 250–264.
50. Yazdani, M., Tuutijärvi, T., Bhatnagar, A., Vahala, R. (2016). Adsorptive removal of arsenic (V) from aqueous phase by feldspars: kinetics, mechanism, and thermodynamic aspects of adsorption. Journal of Molecular Liquids, 214, 149–156.
51. Yew, Y.P., Shameli, K., Miyake, M., Kuwano, N., Khairudin, N.B.B.A., Mohamad, S.E.B. and Lee, K.X. (2016). Green synthesis of magnetite (Fe_3O_4) nanoparticles using seaweed (Kappaphycus alvarezii) extract. Nanoscale Reserch Letters, 11, 276.

Figures

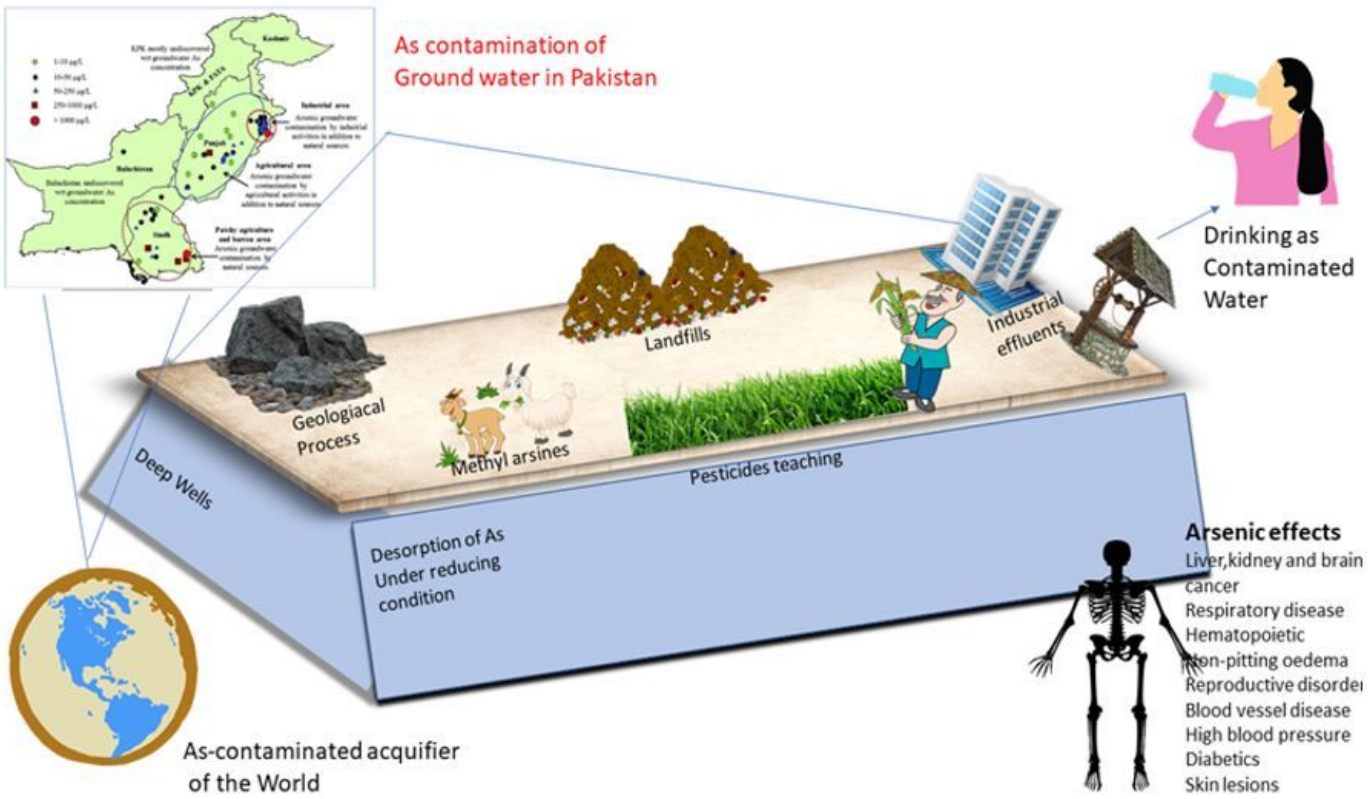

Figure 1

Schematic diagram of arsenic contamination sources.

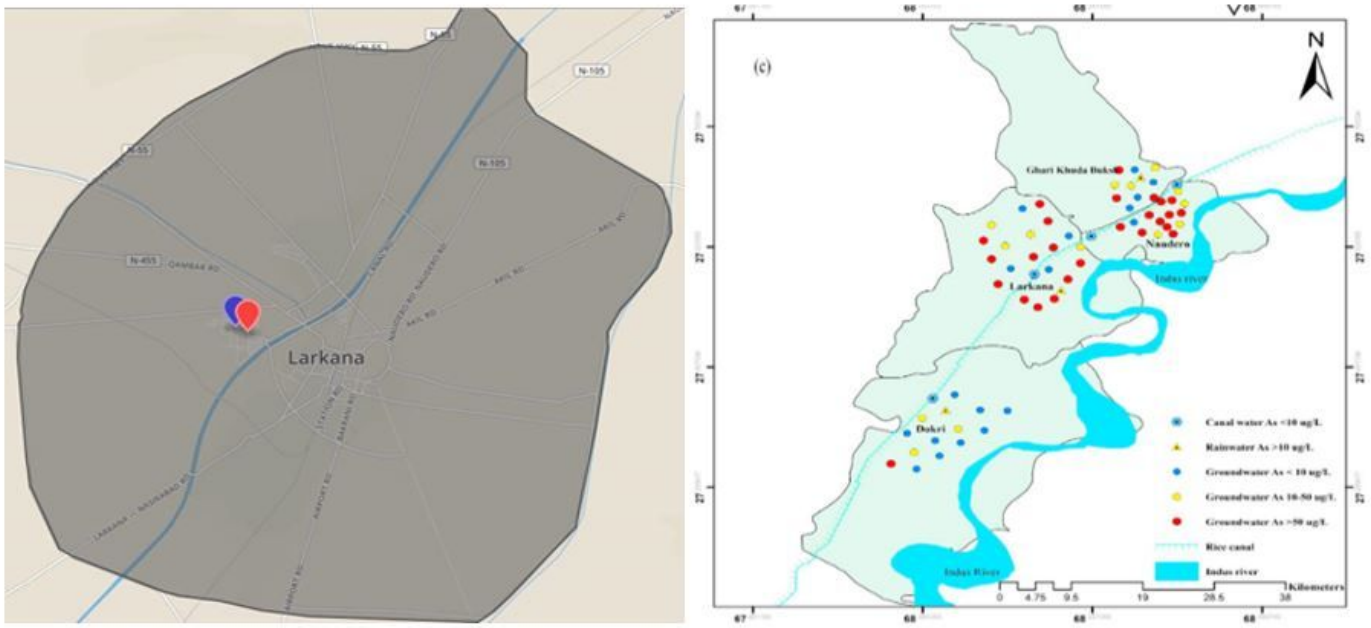

Figure 2

a) Map of Larkana City, Sindh Pakistan and **b)** Source

Figure 3

Removal of arsenic from water samples by iron oxide nanoparticles using ICP-MS.

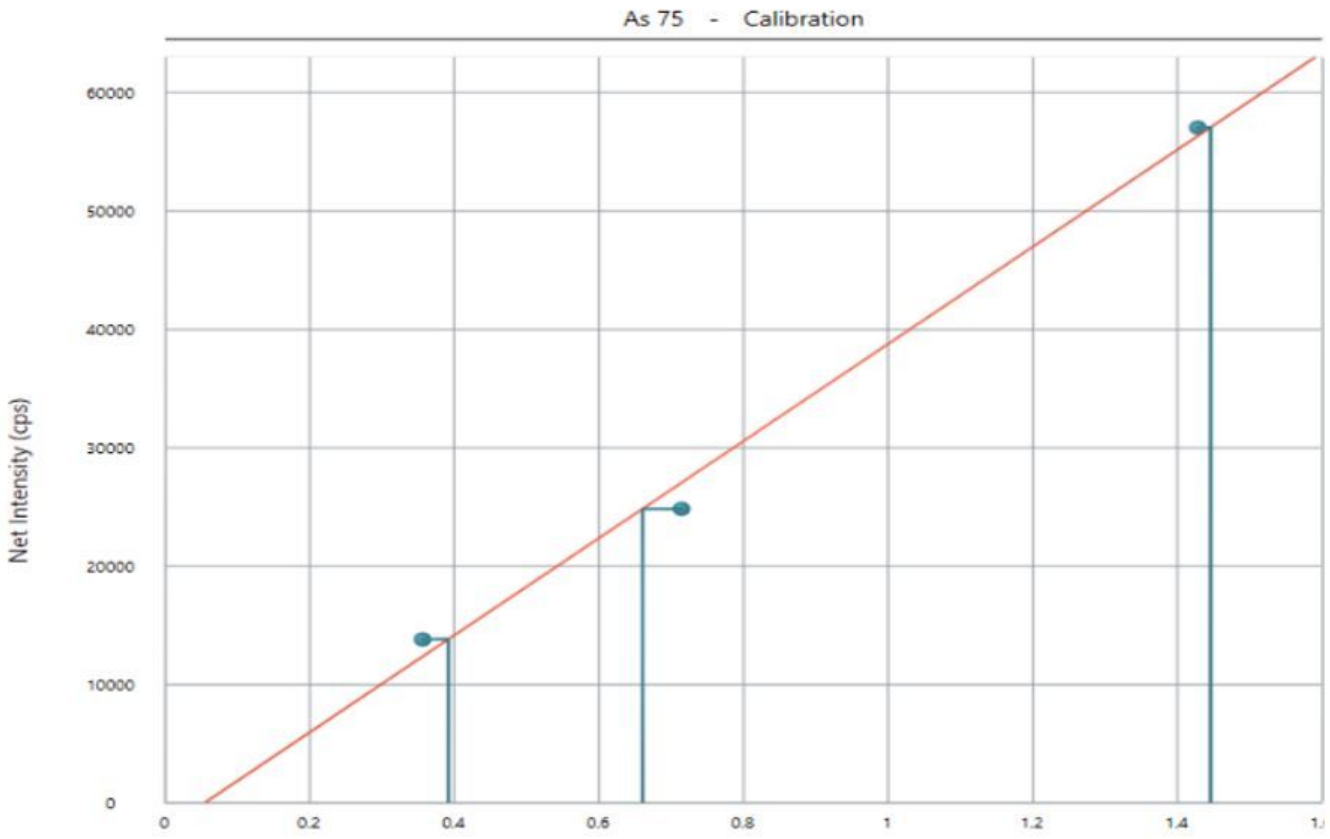

Figure 4

Calibration curve of arsenic for different concentration using ICP-MS.

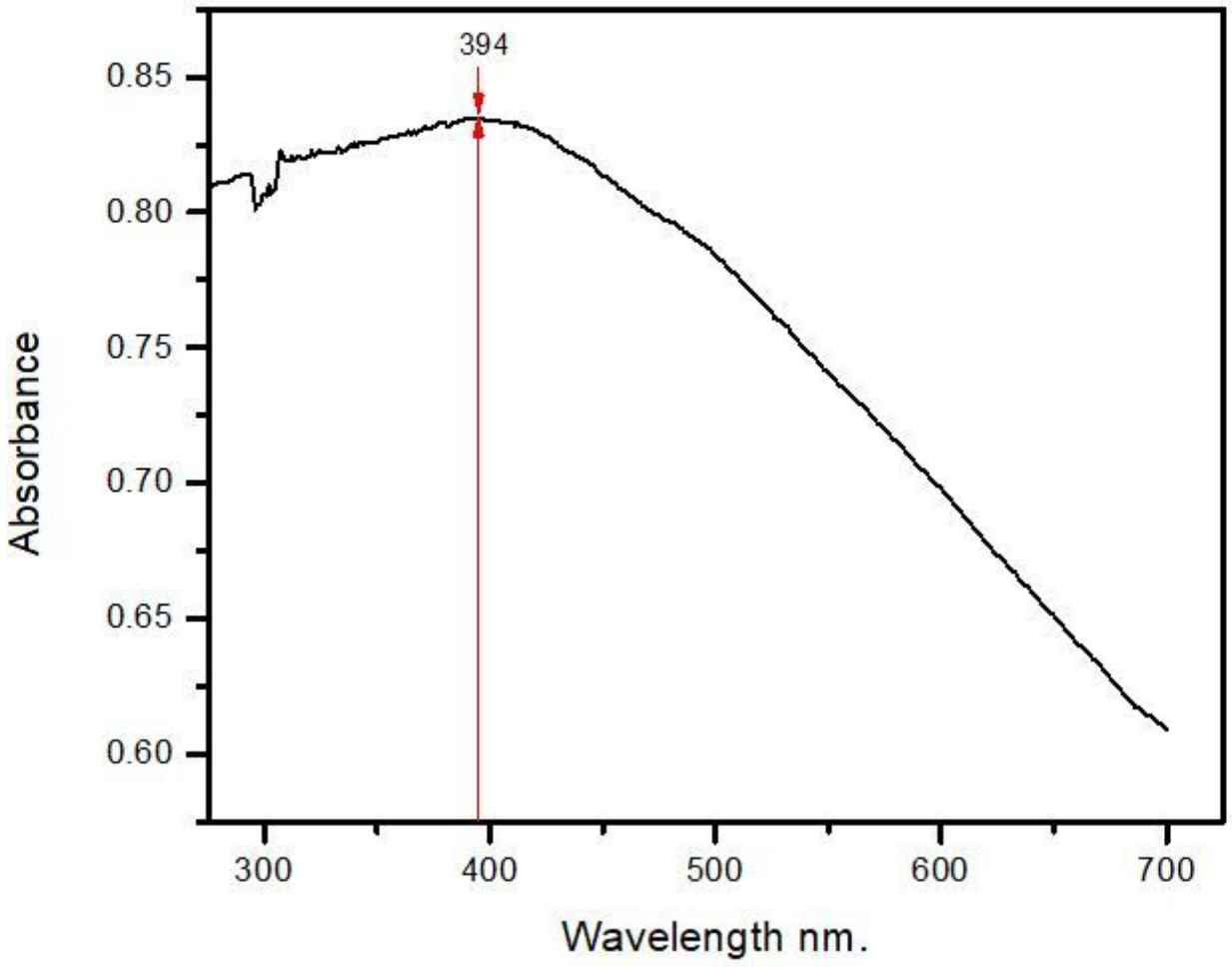

Figure 5

UV-visible spectrum of synthesized iron oxide nano particles.

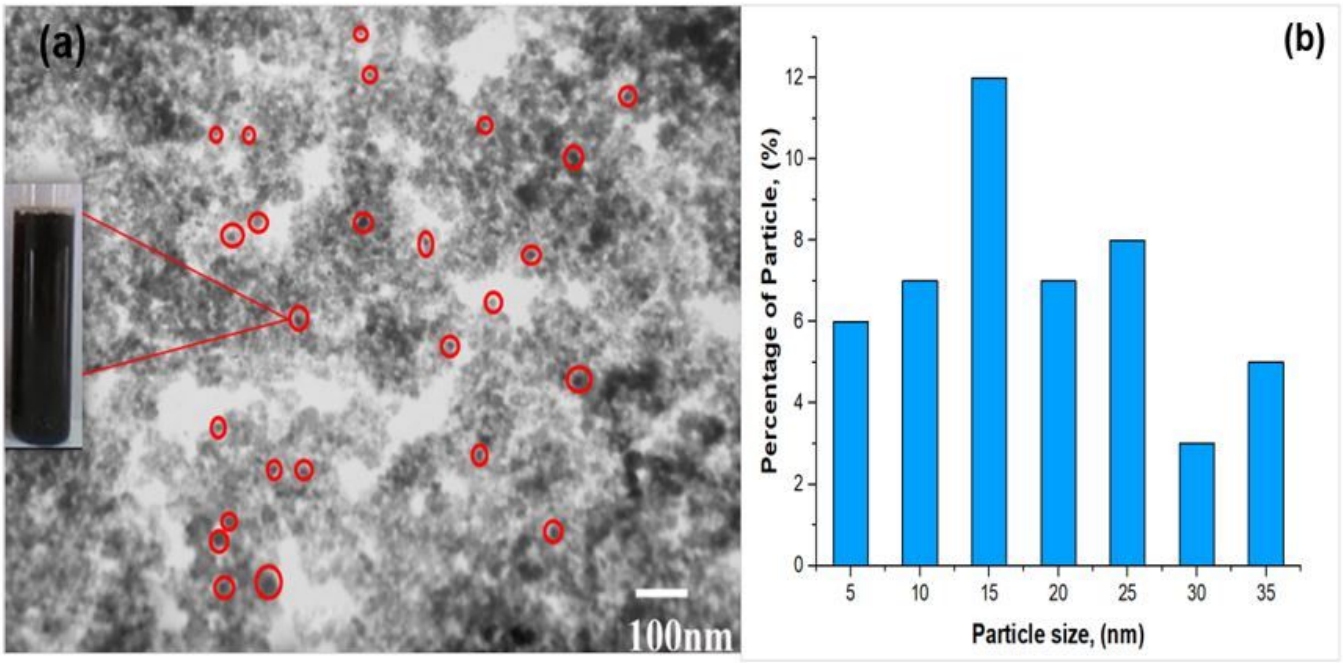

Figure 6

a) TEM image of synthesized iron oxide nanoparticles and b) Particle size distribution of synthesized iron oxide nanoparticles using TEM.

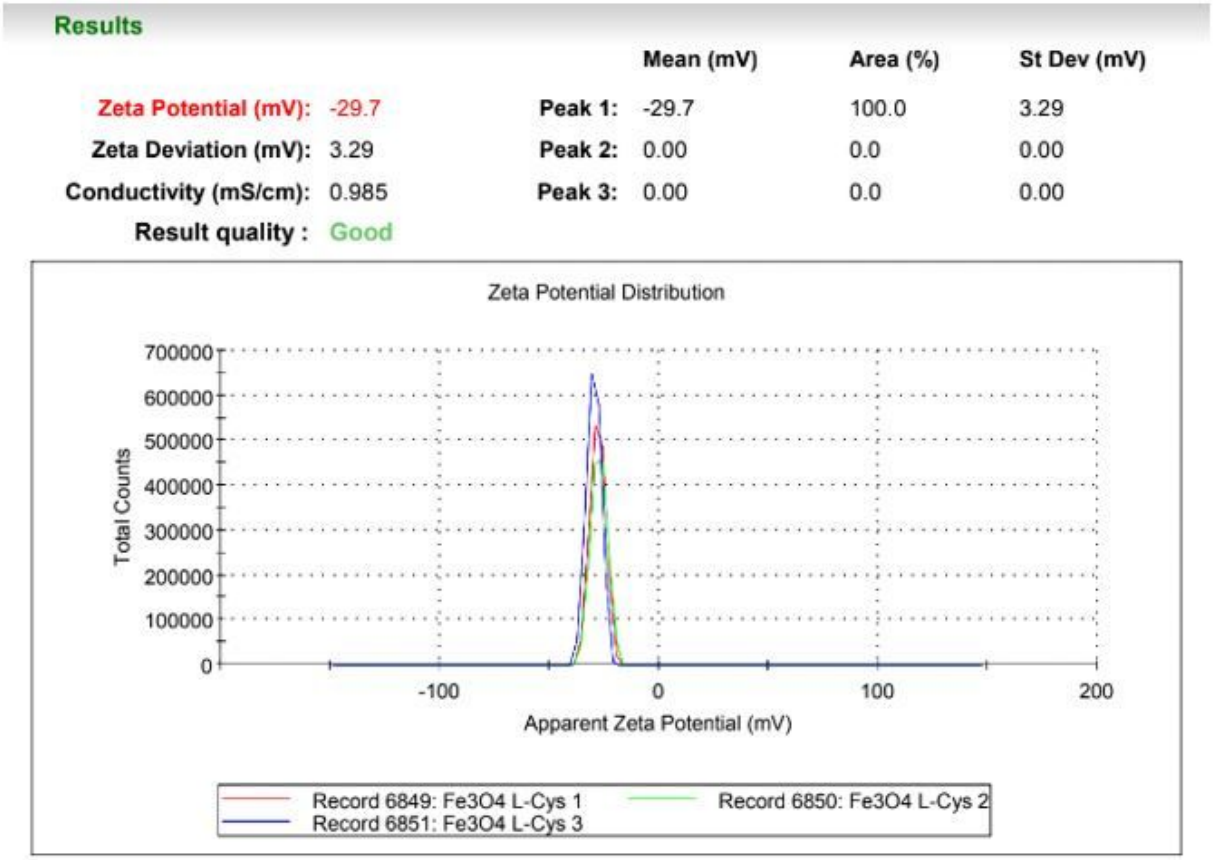

Figure 7

Zeta potential analyzer of synthesized iron oxide nanoparticles.

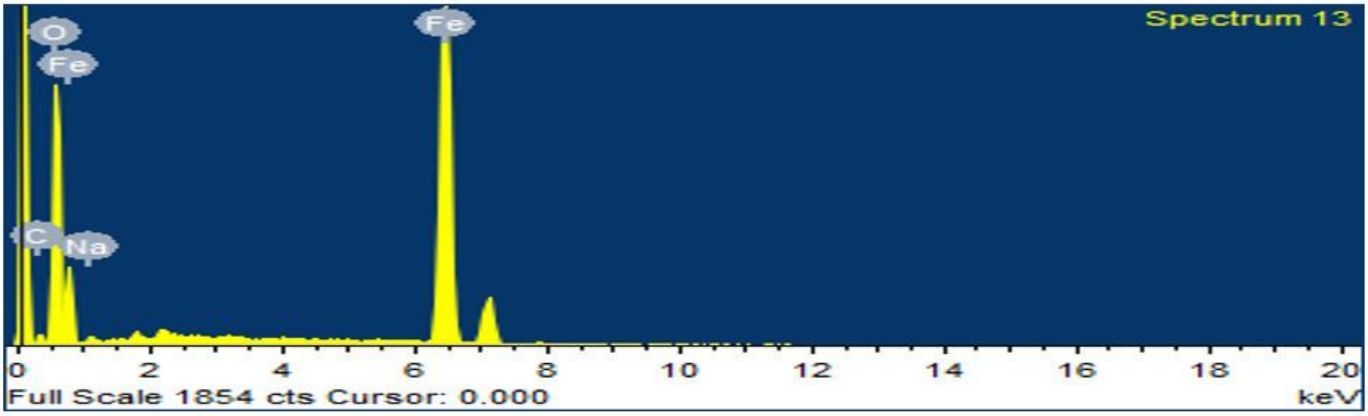

Element	Weight%	Atomic%
C K	4.68	11.85
O K	26.24	49.84
Na K	0.91	1.20
Fe K	68.17	37.10
Totals	100.00	

Figure 8

EDS of synthesized L-cysteine iron oxide nanoparticles.

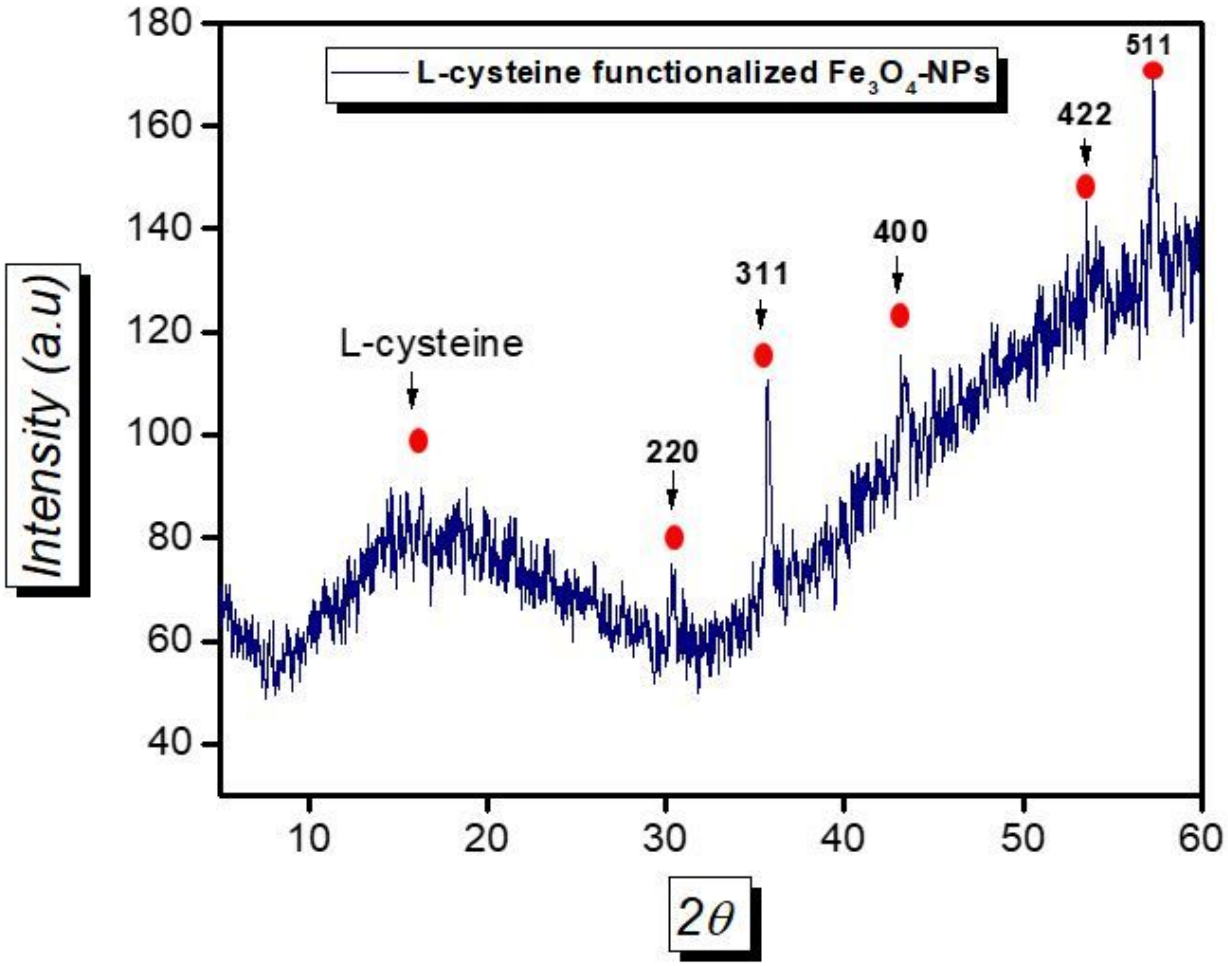

Figure 9

XRD of synthesized L-cysteine iron oxide nanoparticles.

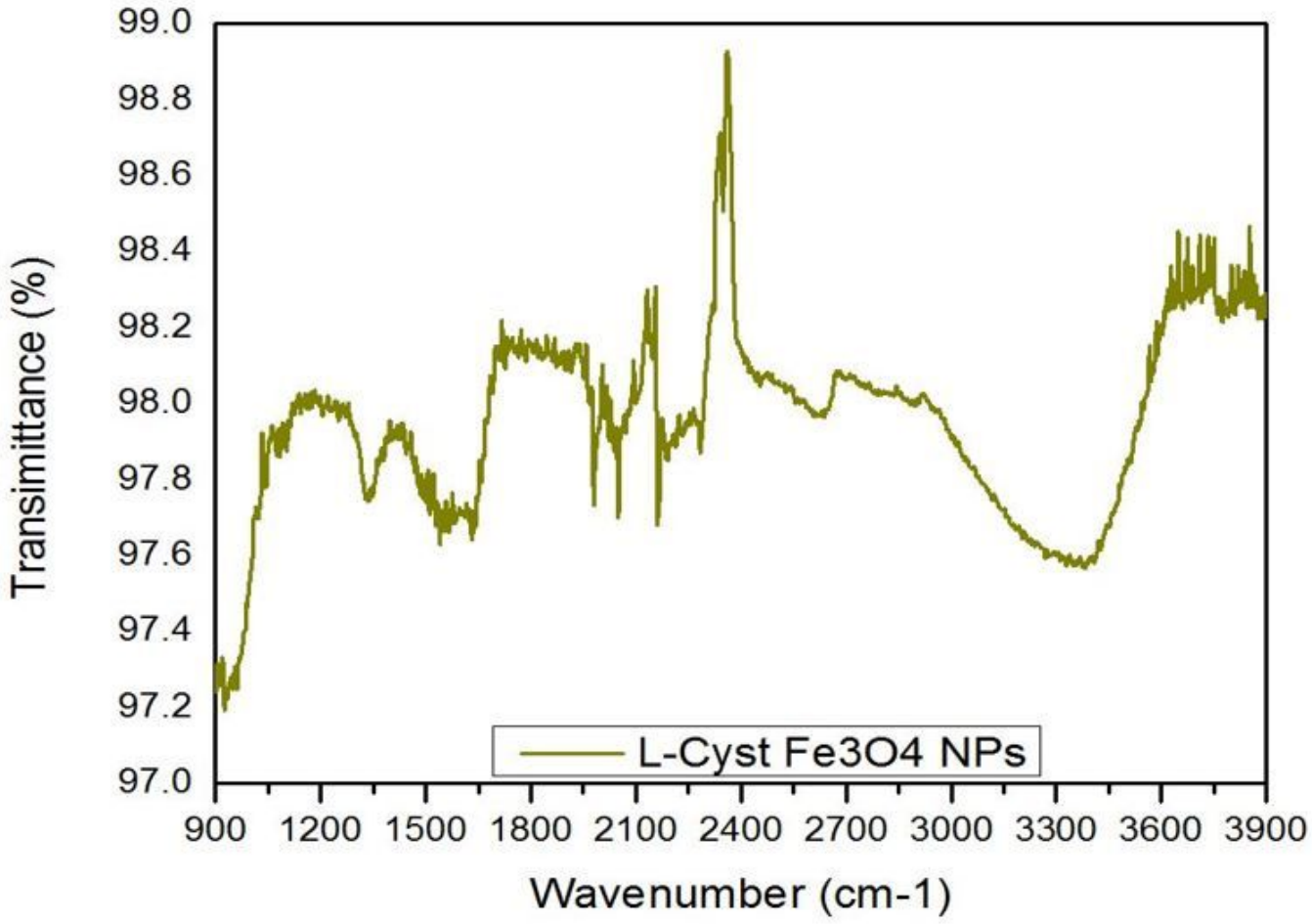

Figure 10

FTIR spectra of synthesized L-cysteine iron oxide nanoparticles.

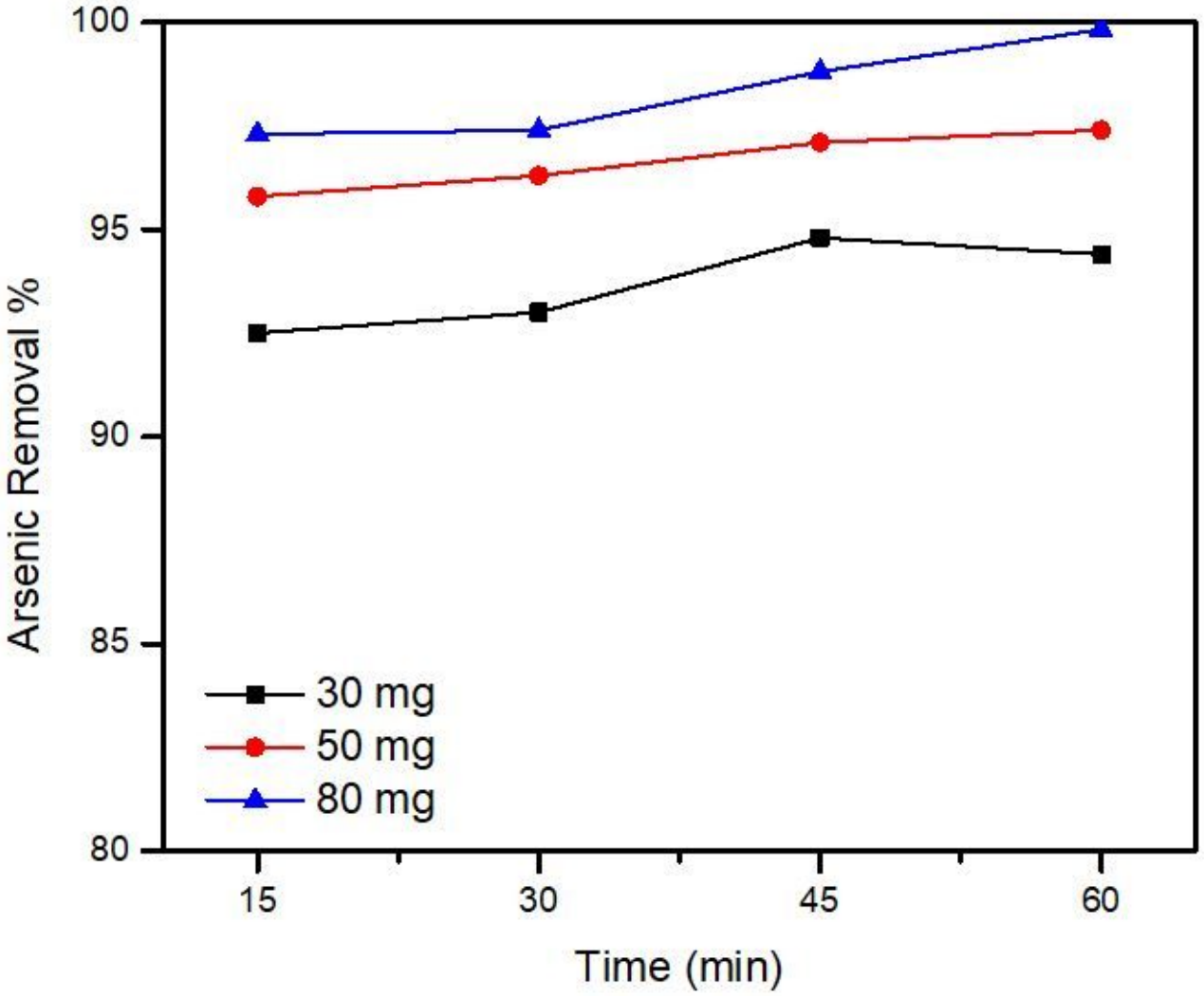

Figure 11

Effect of adsorbent dose for synthesis of L-cysteine iron oxide nanoparticles.

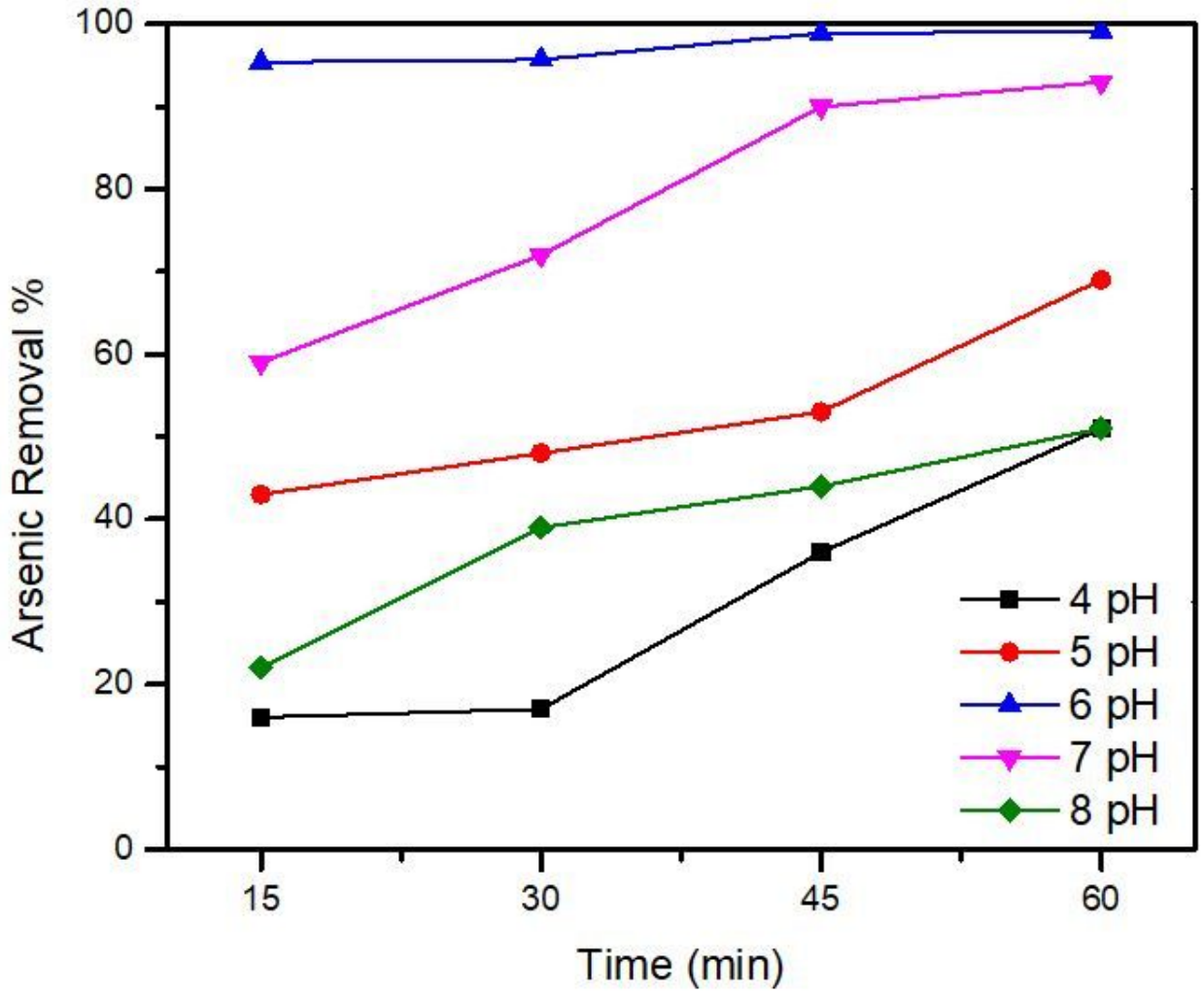

Figure 12

Effect of pH for synthesis of L-cysteine iron oxide nanoparticles.

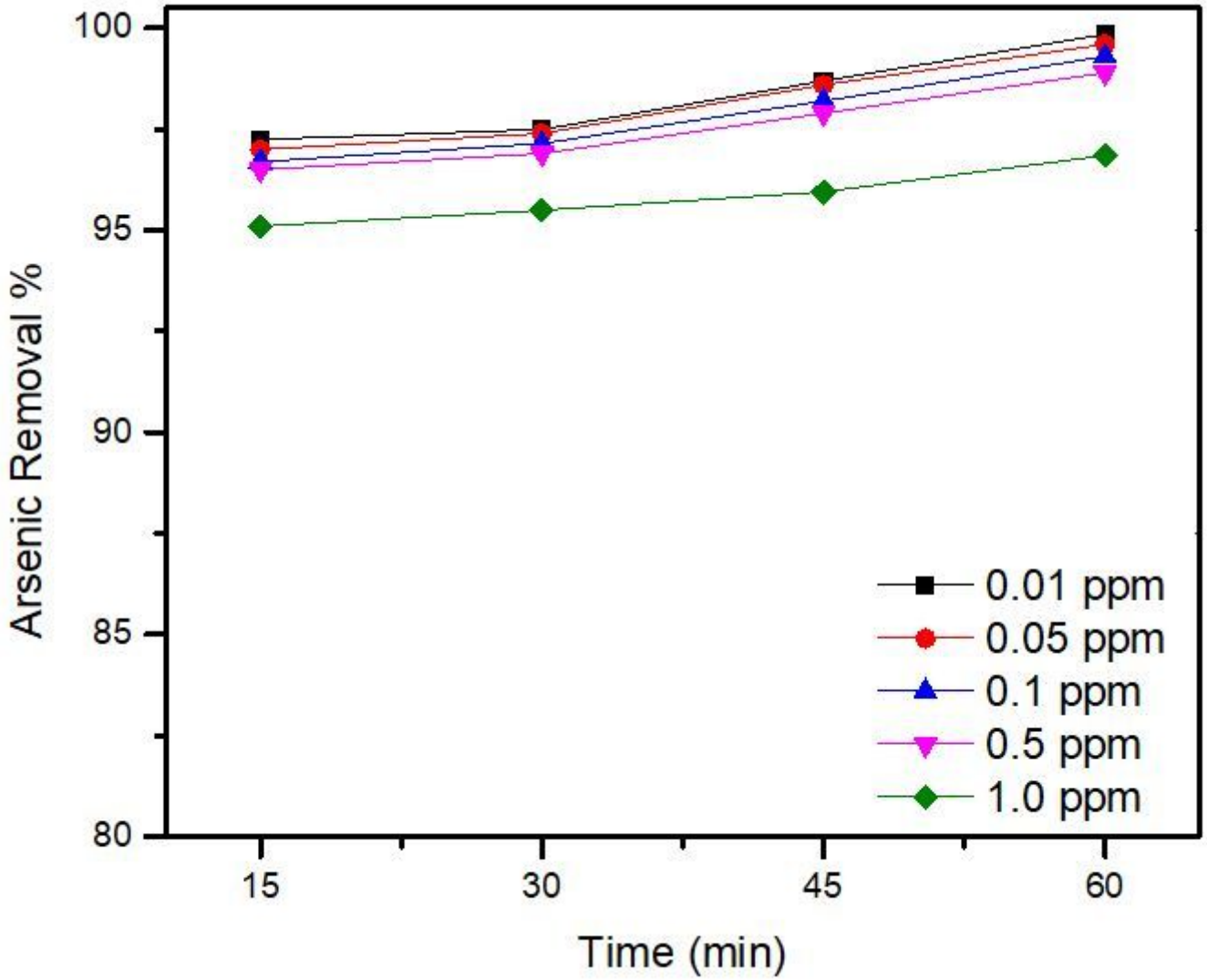

Figure 13

Effect of concentration for synthesis of L-cysteine iron oxide nanoparticles.

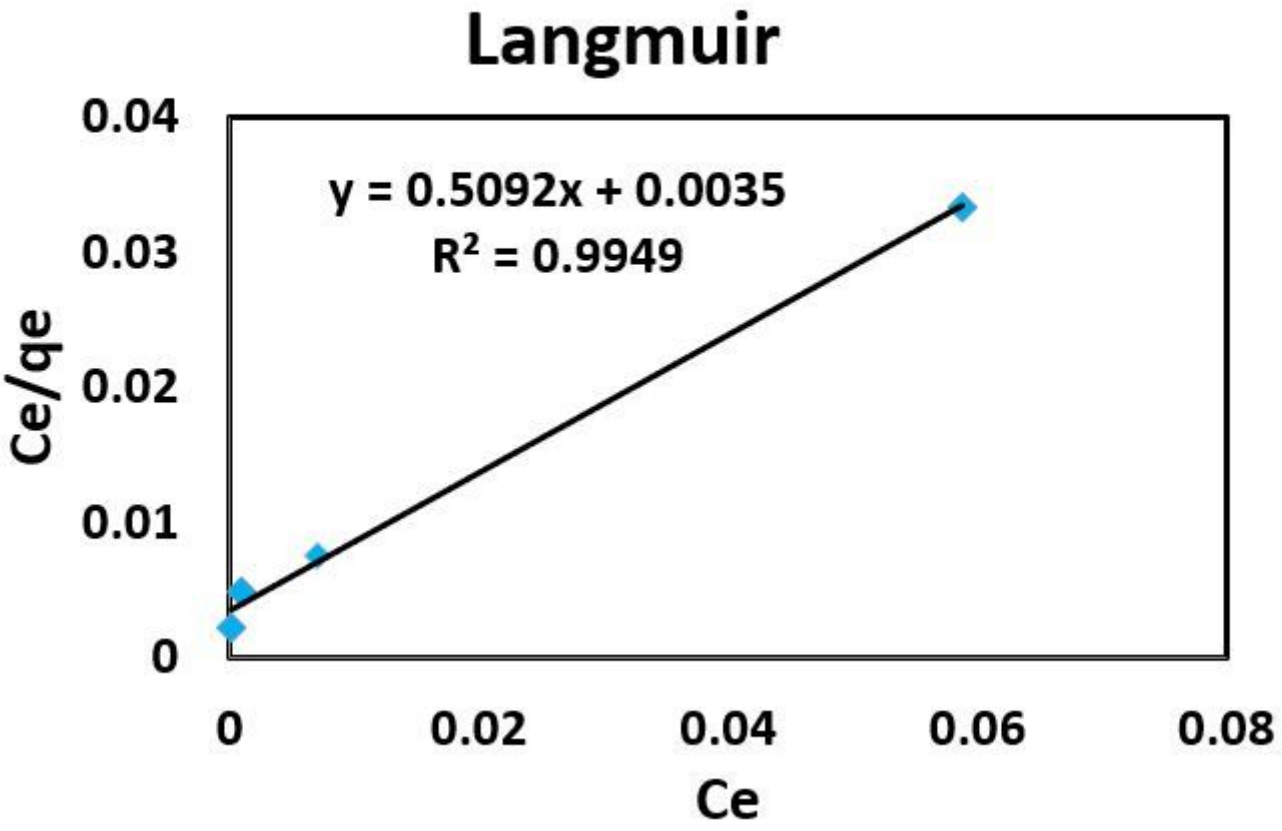

Figure 14

Langmuir model for the removal of arsenic by ICP-MS.

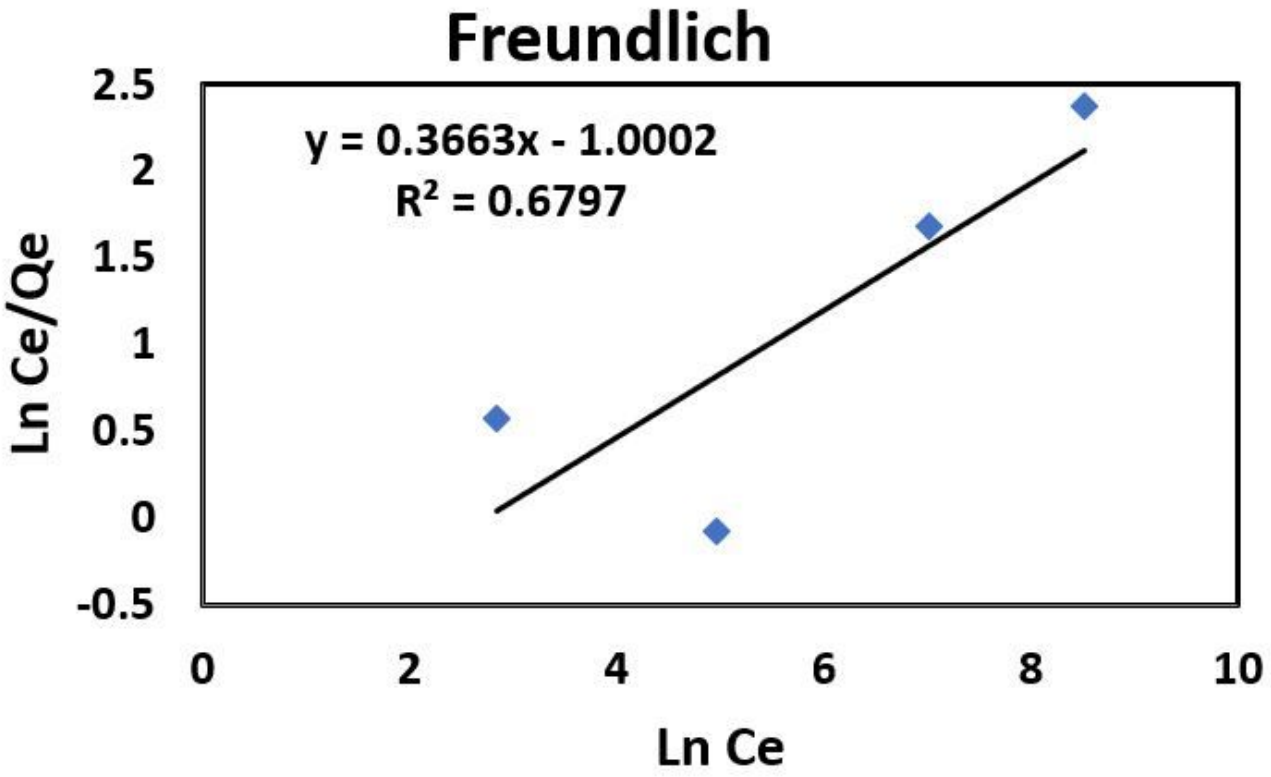

Figure 15

Freundlich model for the removal of arsenic by ICP-MS.

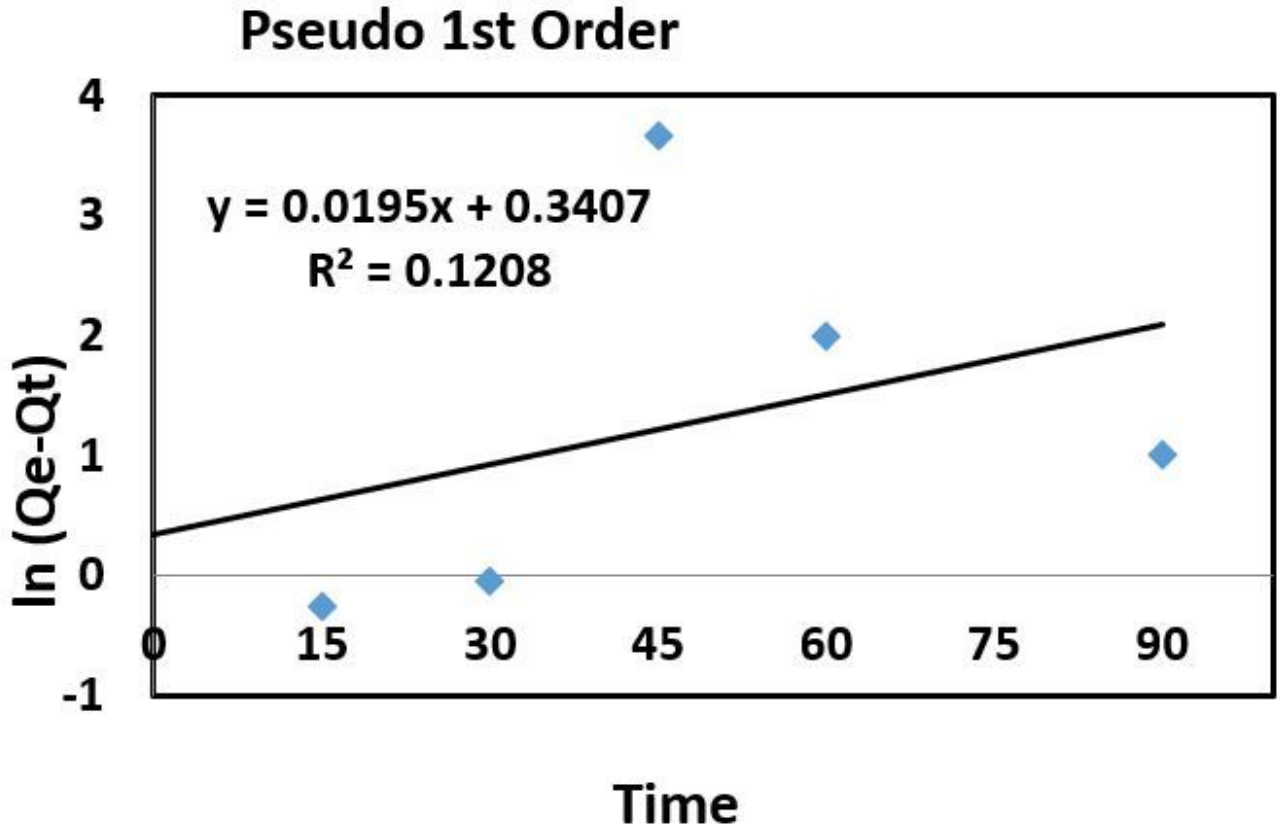

Figure 16

Pseudo 1st order for the removal of arsenic by ICP-MS.

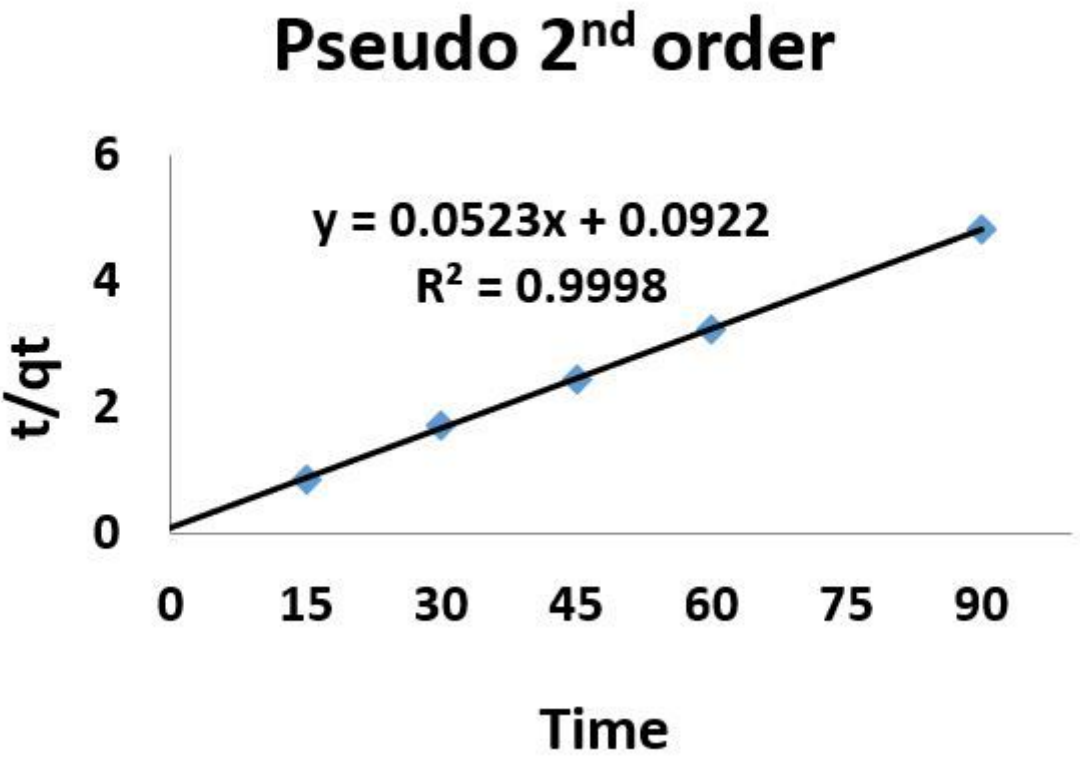

Figure 17

Pseudo 2nd order for the removal of arsenic by ICP-MS.

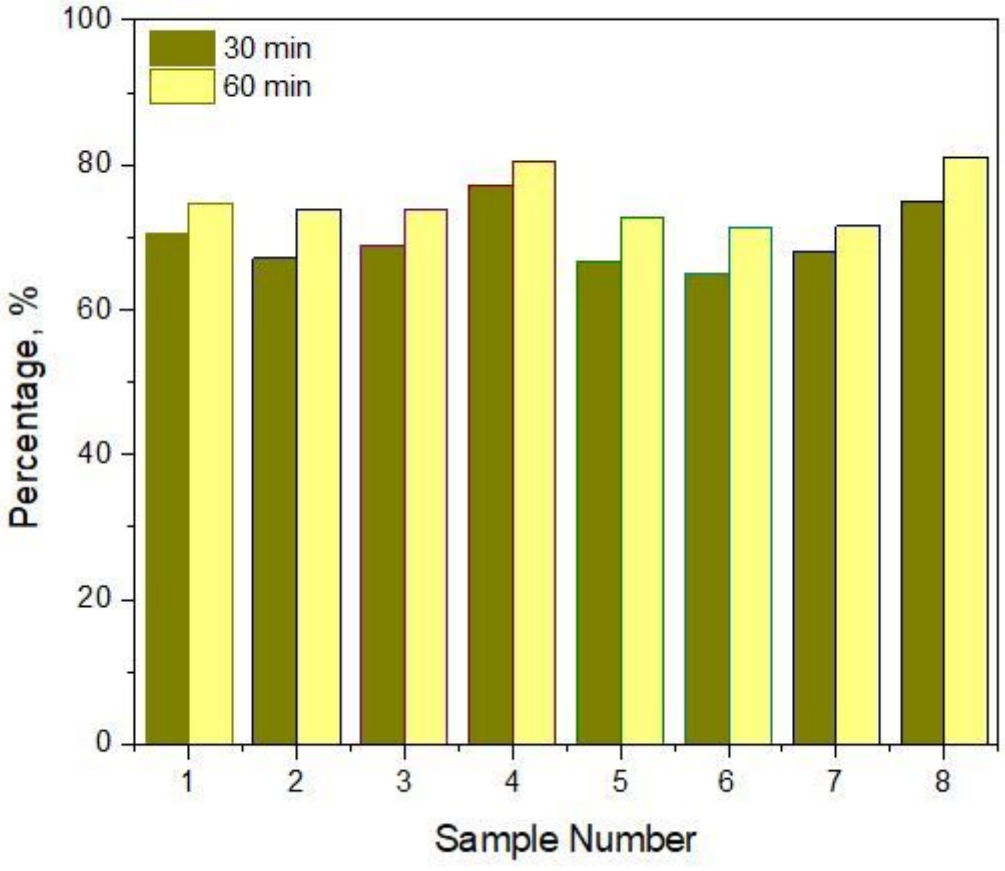

Figure 18

Initial to final concentration for removal of arsenic after 30 and 60min